

Hydrogen transfer reactions of interstellar Complex Organic Molecules

S. Álvarez-Barcia,¹ P. Russ,¹ J. Kästner,¹ and T. Lamberts^{1,2★}

¹*Institute for Theoretical Chemistry, University of Stuttgart, Pfaffenwaldring 55, 70569 Stuttgart, Germany*

²*Current Address: Leiden Institute of Chemistry, Gorlaeus Laboratories, Leiden University, P.O. Box 9502, 2300 RA Leiden, The Netherlands*

Accepted XXX. Received YYY; in original form ZZZ

ABSTRACT

Radical recombination has been proposed to lead to the formation of complex organic molecules (COMs) in CO-rich ices in the early stages of star formation. These COMs can then undergo hydrogen addition and abstraction reactions leading to a higher or lower degree of saturation. Here, we have studied 14 hydrogen transfer reactions for the molecules glyoxal, glycoaldehyde, ethylene glycol, and methylformate and an additional three reactions where CH_nO fragments are involved. Over-the-barrier reactions are possible only if tunneling is invoked in the description at low temperature. Therefore the rate constants for the studied reactions are calculated using instanton theory that takes quantum effects into account inherently. The reactions were characterized in the gas phase, but this is expected to yield meaningful results for CO-rich ices due to the minimal alteration of reaction landscapes by the CO molecules.

We found that rate constants should not be extrapolated based on the height of the barrier alone, since the shape of the barrier plays an increasingly larger role at decreasing temperature. It is neither possible to predict rate constants based only on considering the type of reaction, the specific reactants and functional groups play a crucial role. Within a single molecule, though, hydrogen abstraction from an aldehyde group seems to be always faster than hydrogen addition to the same carbon atom. Reactions that involve heavy-atom tunneling, *e.g.*, breaking or forming a C–C or C–O bond, have rate constants that are much lower than those where H transfer is involved.

Key words: astrochemistry – methods: laboratory: solid state – ISM: molecules

1 INTRODUCTION

Thanks to the unprecedented sensitivity of ALMA the detection and quantification of interstellar complex organic molecules (COM) has become more and more within reach. A complex organic molecule in the context of astrochemistry is loosely defined as a molecule consisting of more than 6 H, C, O, and/or, N atoms. Typical gas-phase abundances of such molecules are only of the order of $< 10^{-8}$ with respect to H₂ (Jørgensen et al. 2012; Halfen et al. 2015; Taquet et al. 2015; López-Sepulcre et al. 2017) with even lower abundances for deuterated species (Belloche et al. 2016). These molecules are currently thought to find their origins in the CO-rich top layers of the grain ice mantle (Boogert et al. 2015) where the H + CO reaction network has been shown to lead to the formation of the parent species formaldehyde, H₂CO, and methanol, CH₃OH (Tielens & Hagen 1982; Hirao et al. 1998; Watanabe & Kouchi 2002; Fuchs et al. 2009). Furthermore, besides hydrogen addition reactions,

also hydrogen abstraction reactions can take place that decrease the number of H atoms on the CO backbone (Nagaoka et al. 2005; Nagaoka et al. 2007). Although it has been suggested that formaldehyde and methanol may desorb from the grain surface and subsequently react in the gas phase to yield more complex species (Bottinelli et al. 2004; Balucani et al. 2015; Taquet et al. 2017), a variety of COMs have been detected in cold interstellar regions (Bacmann et al. 2012; Öberg et al. 2010; Vastel et al. 2014). This indicates that low-temperature surface chemistry can play an important role in the formation of larger species.

In fact the H + CO reaction network has evolved into a network where carbon-carbon bonds can be formed via radical-radical reactions between the ‘fundamental’ radicals that are created as intermediates, *i.e.*, HCO, CH₂OH, and CH₃O. Most of these reactions have been studied experimentally in various ways (Fedoseev et al. 2015; Butscher et al. 2015; Chuang et al. 2016; Fedoseev et al. 2017; Chuang et al. 2017; Butscher et al. 2017) and they have also been proposed by and are included in a number of astrochemical model studies (Garrod et al. 2008; Woods et al. 2012;

★ E-mail: a.l.m.lamberts@lic.leidenuniv.nl

Coutens et al. 2018). Similar conclusions are also supported by observational work for specific species (Rivilla et al. 2017; Li et al. 2017). Despite this significant amount of investigations, relatively little is known about the reaction rate constants at low temperature, while these are the crucial parameters needed to constrain modeling studies.

Here we focus on hydrogen addition and abstraction reactions of species with two carbon atoms and two oxygen atoms, *i.e.*, methylformate, glyoxal, glycoaldehyde, and ethylene glycol (Section 3.1). Several other reactions are discussed as well where a C–C or C–O bond is formed via an over-the-barrier reaction between an CH_nO radical and formaldehyde (Section 3.2). Finally, we provide an overview of reaction rate constants previously calculated for the CO + H network involving both formaldehyde and methanol (Andersson et al. 2011a; Goumans & Kästner 2011; Goumans 2011b; Song & Kästner 2017) (Section 3.3). Low-temperature reaction rate constants have been calculated for the first time using instanton theory and serve as an order of magnitude estimate implementation in astrochemical models. We will also comment on the possibility to generalize rate constants based only on the type of reaction.

2 COMPUTATIONAL DETAILS

Two different levels of theory have been used throughout this study in order to balance the computational cost and chemical accuracy. All calculated activation and reaction energies, as well as the rate constants have been calculated with density functional theory (DFT). In particular, the functional MPWB1K combined with the basis set def2-TZVP has been used. The accuracy of the activation energies or barrier heights is ensured by benchmarking these values to a better level of theory, namely CCSD(T)-F12/VTZ-F12.

Optimizations of the stationary points, corresponding energies, and spin densities were computed at the MPWB1K/def2-TZVP level (Zhao & Truhlar 2004; Weigend & Ahlrichs 2005; Weigend 2006). Geometry optimizations (minima and transition states) were done with DL-FIND (Kästner et al. 2009) in ChemShell (Sherwood et al. 2003; Metz et al. 2014). For the electronic structure computations (energies, gradients, and Hessians) Gaussian 09 (M. J. Frisch 2009) has been employed. SCF cycles were stopped when the convergence, as defined in G09, reached 1×10^{-9} Hartree. A pruned (99 590) grid (ultrafine grid) was employed, having 99 radial shells and 590 angular points per shell.

The MPWB1K functional has been previously benchmarked in order to predict the correct bond dissociation energy of methyl formate (MF), for which accurate results were obtained (Li et al. 2016). Furthermore, MPWB1K was developed to take into account weak interactions such as those found in the pre-reactive complexes treated here. In order to confirm the use of this functional for the current study, single point energy calculations at the RHF-UCCSD(T)-F12/VTZ-F12//MPWB1K/def2-TZVP level (Knowles et al. 1993, 2000; Deegan & Knowles 1994; Adler et al. 2007; Knizia et al. 2009; Peterson et al. 2008b) were carried out and are discussed in Appendix A.

The instanton method based on Feynman path integral theory using the semiclassical approximation was used to compute the reaction rate constants (Langer 1967, 1969;

Miller 1975; Coleman 1977; Callan Jr. & Coleman 1977; Gildener & Patrascioiu 1977; Affleck 1981; Coleman 1988; Hänggi et al. 1990; Benderskii et al. 1994; Messina et al. 1995; Richardson & Althorpe 2009; Kryvohuz 2011; Althorpe 2011; Rommel et al. 2011; Rommel & Kästner 2011; Kryvohuz 2014; Richardson 2016). For a given temperature, it provides the most probable tunnelling path, the instanton, which connects the reactant and product valleys of the potential energy surface. Instanton theory is applicable whenever the temperature is low enough for the instanton to spread out. At higher temperatures, the instanton collapses to a point which renders the theory inapplicable. For most barriershapes this collapse happens at the crossover temperature T_c (Gillan 1987; Álvarez-Barcia et al. 2014),

$$T_c = \frac{\hbar \Omega}{2\pi k_B} \quad (1)$$

with Ω being the the absolute value of the imaginary frequency corresponding to the transition mode and k_B corresponding to Boltzmann’s constant. T_c qualitatively indicates at which temperature the reaction is dominated by tunneling ($T < T_c$) or by the thermal activation ($T > T_c$).

Instanton paths were optimized via a quasi Newton–Raphson method (Rommel et al. 2011; Rommel & Kästner 2011). Energies, gradients, and Hessians were provided by Gaussian 09, but instanton optimizations are done in DL-FIND. The instanton path was discretised using 80 images, except for reactions MF3 and MF4 where 158 images were employed at $T \leq 100$ K and 314 images for MF4 at 75 K.

This study focuses on unimolecular rate constants, *i.e.*, on the Langmuir–Hinshelwood mechanism. Both reactants are adsorbed on the surface, approach each other via diffusion and form a pre-reactive complex (PRC) on the surface. This PRC can then decay to yield the reaction products via a unimolecular process. It has been shown in the recent literature that often gas-phase calculations of stationary points offer a reasonably accurate approach for representing the very same reactions on an ice surface. This even holds for ices composed of water molecules as typical changes of the activation energy are roughly only 1–2 kJ/mol (Rimola et al. 2014; Song & Kästner 2017; Lamberts 2018). However, in particular cases, larger energy differences may be found (Lamberts & Kästner 2017b) and to which extent surface molecules may affect the binding orientation is currently unclear. Finally, adsorption on a surface is simulated by keeping the rotational partition function constant between the reactant and transition state. For more information regarding this approach the reader is referred to Meisner et al. (2017) and Lamberts & Kästner (2017a).

3 RESULTS

We simulated a total of 14 reactions revolving around the molecules glyoxal (GX), glycoaldehyde (GA), ethylene glycol (EG), and methyl formate (MF), an additional three reactions where reactions of CH_nO fragments with H_2CO are involved (FAR), and discuss the results in the light of the 6 previously studied reactions with carbon monoxide (CO), formaldehyde (FA), and methanol (ME). To structure the analysis, the reactions are labeled according to their type, except for the FARn series:

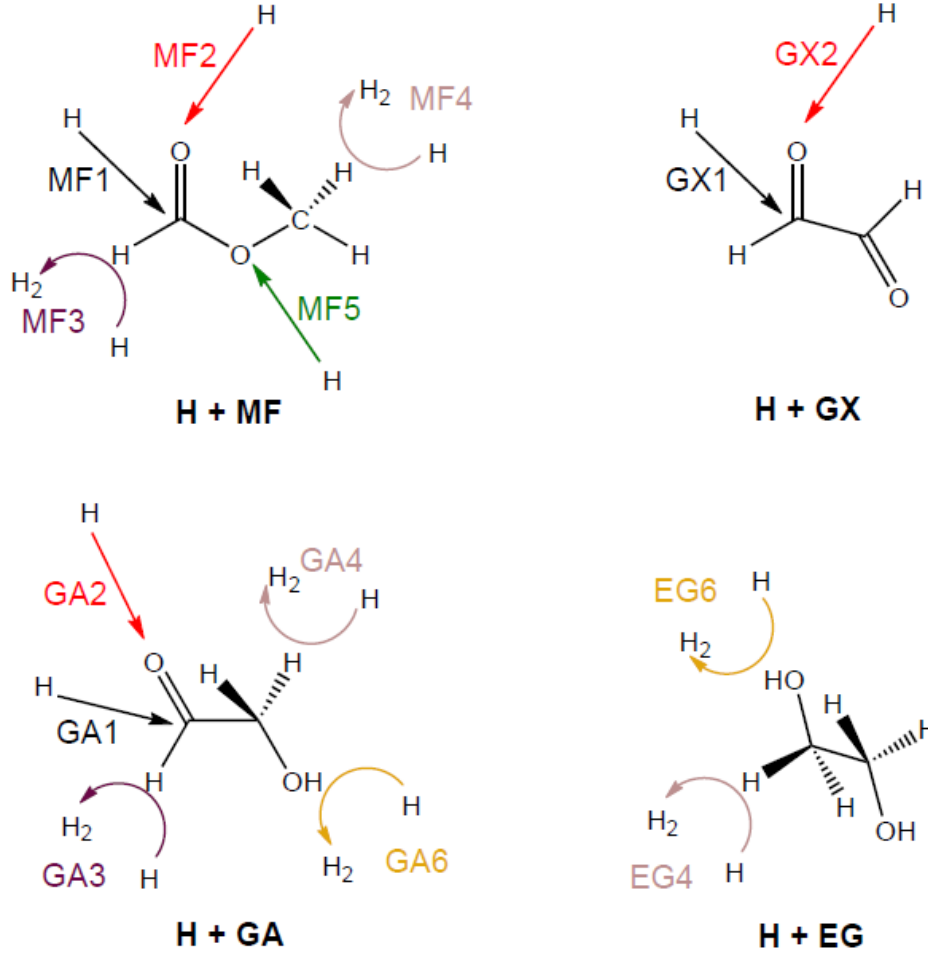


Figure 1. Schematic representation of the reactions shown in section 3.1. MF, GX, GA and EG, correspond to methylformate, glyoxal, glycoaldehyde, and ethylene glycol, respectively.

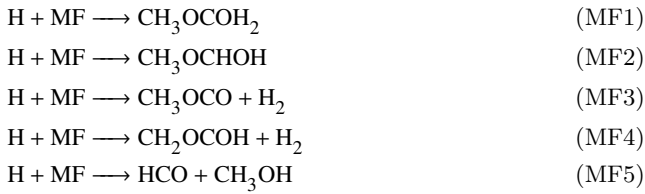
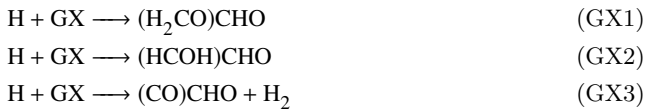
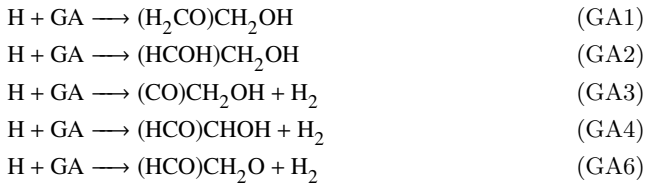
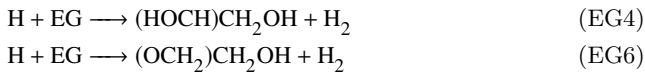
- 1) H addition to aldehyde carbon – MF, GX, GA, CO, FA
- 2) H addition to aldehyde oxygen – MF, GX, GA, FA
- 3) H abstraction from aldehyde carbon – MF, GX, GA, FA
- 4) H abstraction from methyl group – MF, EG, ME
- 5) H addition to etheric oxygen – MF
- 6) H abstraction from alcohol oxygen – GA, EG, ME

Note that we expect all reactions studied and discussed here to take place in an environment where carbon monoxide, CO, is the main component of the ice mantle. Due to the general weak interactions of this molecule, we expect that the activation energies calculated here in the gas phase will be similar to those in the presence of a CO environment. For instance for the reactions $H + CO$ and $H + H_2CO$ this has been confirmed by [Rimola et al. \(2014\)](#). Therefore, the values presented here are thought to be a good representation of the situation in the interstellar medium.

3.1 Reactions with MF, GX, GA, and EG

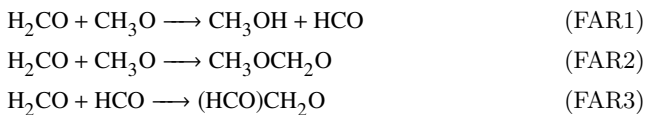
Activation energies for the reactions described in this Section and in Section 3.2 can be found in Table 1. Crossover temperatures (T_c) as an indication of the importance of tunneling, and the calculated low-temperature rate constants are

presented as well. A schematic representation of the reactions with methylformate, glyoxal, glycoaldehyde, and ethylene glycol is given in Figure 1. The temperature-dependence of the calculated rate constants is depicted in Figs. 2–6. The reaction of the hydrogen atom with methylformate has been studied in order to determine if it is an efficient destruction channel. The addition and abstraction reactions of H with glyoxal, glycoaldehyde, and ethylene glycol serve to study the sequential hydrogenation steps. In this way the same reaction type (see above) can be compared between various molecules, and it can be determined whether or not addition is faster than abstraction. Note that the reaction abstracting a hydrogen atom from glyoxal (GX3) could not be studied, because according to the benchmark study the most accurate value for the activation energy cannot be validated: the difference between the DFT and CCSD(T)-F12 value is too large and moreover multireference effects prevent the CCSD(T)-F12 value from being trusted.

Reactions with methylformate (MF)*Reactions with glyoxal (GX)**Reactions with glycoaldehyde (GA)**Reactions with ethylene glycol (EG)***3.2 Reactions between FA and CH_nO**

Although the COMs discussed above have been proposed to be formed mainly through radical-radical reactions, reactions between a neutral and radical species may also lead to the formation of a C–C or C–O bond. The reactions between H₂CO and CH₃O or HCO (Butscher et al. 2017) are therefore studied as well in order to compare their efficiency to other radical-neutral reactions as well as to fast barrierless radical-radical reactions.

Reactions FAR1 and FAR2 are in direct competition with each other, see also Fig. 7.

**3.3 Reactions with CO, FA, and ME**

Prior to discussing hydrogen transfer reactions in COMs, this Section summarizes previous theoretical studies related to the H + CO reaction network for cases where calculations have also been performed with instanton theory. The main results, in terms of activation energy and reaction rate constant from those studies are listed in Table 2.

Table 1. Activation energies with respect to the pre-reactive complexes computed at the MPWB1K/def2-TZVP level with ($\Delta E^{0,\ddagger}$) and without (ΔE^\ddagger) ZPE correction. Crossover temperatures (T_c) and rate constants (k at 75 K unless indicated otherwise) are also included.

	ΔE^\ddagger (kJ mol ⁻¹)	$\Delta E^{0,\ddagger}$ (kJ mol ⁻¹)	T_c (K)	k (75 K) s ⁻¹
H + MF				
MF1	38.1	41.2	262.2	3.6×10^{-1}
MF2	59.0	59.9	400.4	1.7
MF3	46.6	38.1	365.8	3.4^a
MF4	51.2	42.8	345.1	1.1×10^{-1}
MF5	146.0	149.9	496.7	3.8×10^{-33}
H + GX				
GX1	15.1	15.1	179.9	9.6×10^6
GX2	29.8	31.7	298.9	1.8×10^3
H + GA				
GA1	19.0	20.8	203.4	2.8×10^5
GA2	38.5	39.8	342.5	2.8×10^2
GA3	24.3	14.6	317.6	6.8×10^7
GA4	27.3	20.6	333.5	2.6×10^4
GA6	55.8	46.2	405.2	9.6×10^{-1}
H + EG				
EG4	28.4	19.3	303.3	3.5×10^6
EG6	54.1	42.2	406.3	2.1×10^{3b}
FAR _n				
FAR1	30.6	22.2	336.6	2.0×10^{3c}
FAR2	44.8	48.5	151.9	4.6×10^{-9d}
FAR3	19.9	24.5	58.3	3.9×10^{-11c}

^a at 80 K

^b at 90 K

^c at 50 K

^d at 65 K

Table 2. Activation energies including ZPE ($\Delta E^{0,\ddagger}$) and unimolecular rate constants (k) obtained from literature values.

	$\Delta E^{0,\ddagger}$ (kJ/mol)	k s ⁻¹
H + CO		
CO1	$12.4 + \sim 1.2^a$	2.1×10^5 at 5 K [1]
H + FA		
FA1	15.8 - 17.9	$1.5 \times 10^5 - 2.0 \times 10^6$ at 70 K [2]
FA2	43.3 - 47.1	$4.0 \times 10^1 - 9.0 \times 10^1$ at 75 K [2]
FA3	20.5 - 25.2	$4.0 \times 10^5 - 1.0 \times 10^6$ at 70 K [2]
H + ME		
ME4	30.2	– [3]
ME6	46.4	– [3]

^a ZPE calculated in this work (CCSD(T)-F12/VTZ-F12)

[1] Andersson et al. (2011b) [2] Song & Kästner (2017)

[3] Goumans & Kästner (2011)

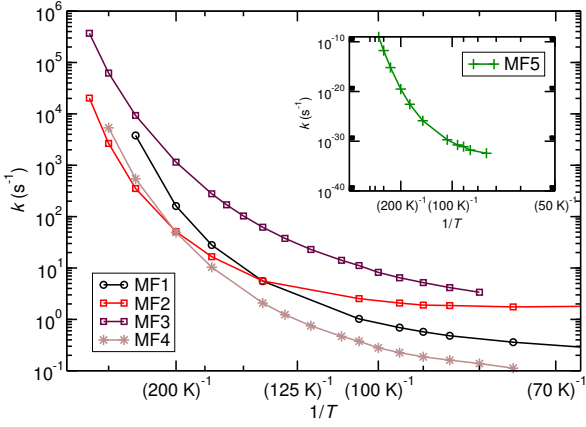


Figure 2. Unimolecular rate constants (in s^{-1}) calculated with instanton theory for the methylformate (MF) + H reactions.

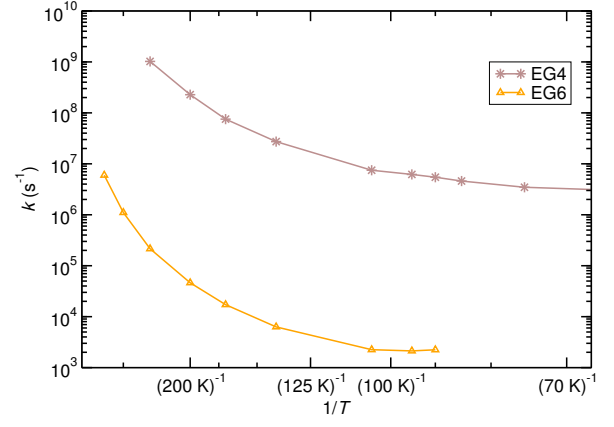


Figure 5. Unimolecular rate constants (in s^{-1}) calculated with instanton theory for the ethylene glycol (EG) + H reactions.

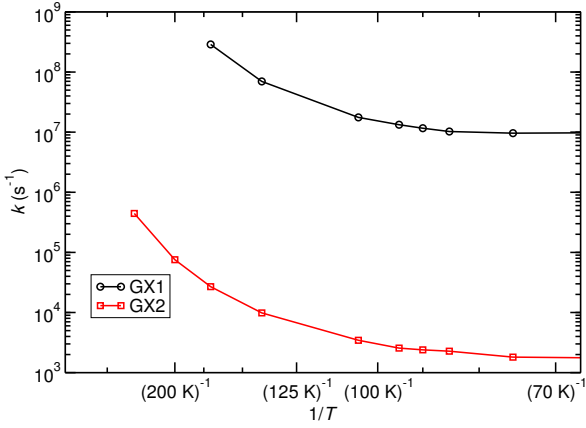


Figure 3. Unimolecular rate constants (in s^{-1}) calculated with instanton theory for the glyoxal (GX) + H reactions.

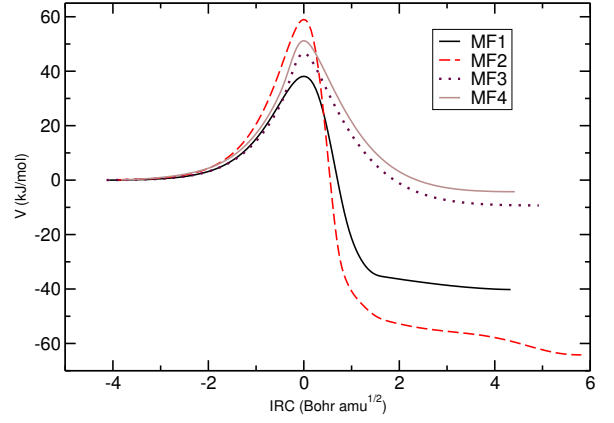


Figure 6. Intrinsic reaction coordinates for reactions MF1 - MF4.

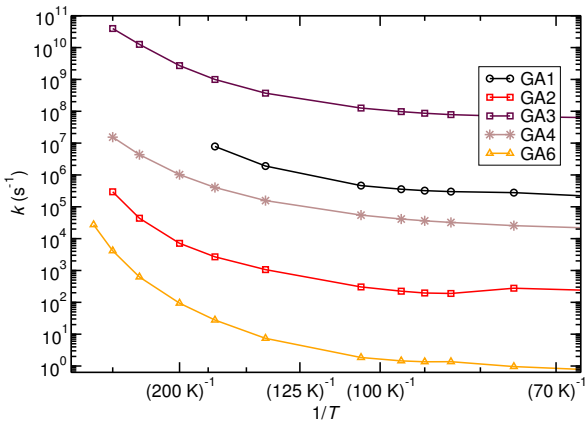


Figure 4. Unimolecular rate constants (in s^{-1}) calculated with instanton theory for the glycoaldehyde (GA) + H reactions.

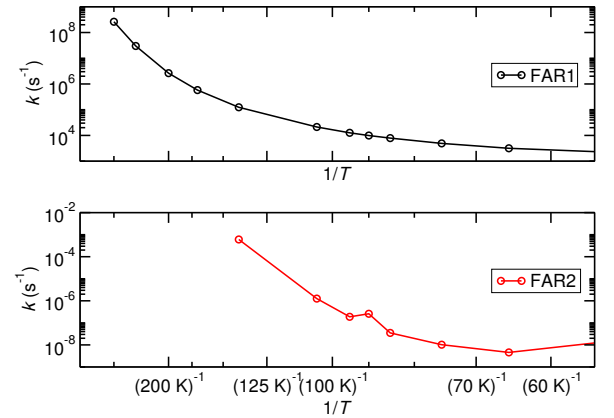
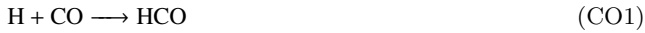


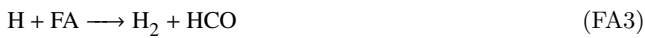
Figure 7. Unimolecular rate constants (in s^{-1}) calculated with instanton theory for the reactions of formaldehyde with CH_nO fragments (FARn).

Reaction with CO

Unimolecular rate constants for the H + CO system have been theoretically calculated by [Andersson et al. \(2011b\)](#), using a PES previously obtained by [Keller et al. \(1996\)](#):

*Reactions with FA*

The reaction of H and H₂CO (H + FA) has been theoretically studied by both [Goumans \(2011a\)](#) and [Song & Kästner \(2017\)](#).

*Reactions with ME*

The abstraction of H on the methanol (ME) methyl group has been studied theoretically by [Goumans & Kästner \(2011\)](#).

**4 DISCUSSION****4.1 Hydrogen addition and abstraction reactions**

For most of the reactions, the rate constants level off at a given temperature, especially below 80 K.

The reactions of the hydrogen atom with methylformate overall have the highest activation energies, indicating that MF is quite stable with respect to attack by a H radical. Reaction MF5 is a special case, where a C–O bond is being broken while an O–H bond is formed, which is most likely the reason for the corresponding activation energy, or high barrier.

Comparing between the various reaction types, Figures 2 and 4 show that the H abstractions from the H of the HC=O group (type 3) occur with high reaction rate constants. The H abstraction from the -OH group (type 6), on the other hand, appears to be very unfavourable with barriers larger than ~50 kJ/mol (Figures 4 and 5). This is consistent with previous results obtained for the reaction between hydrogen and methanol. The barrier between reactions ME4 and ME6 differs by 16 kJ/mol, in line with the experimental work of [Chuang et al. \(2016\)](#) and [Nagaoka et al. \(2007\)](#).

Generalizing reaction types 1, 2, and 4 is not trivial. The activation energies for type 1 are always lower than those for type 2, when compared within the same molecule (FA, MF, GX, and GA). For instance the formation of CH₃O is preferred over the formation of CH₂OH, contrary to the findings of [Butscher et al. \(2015\)](#), but in line with those of [Chuang et al. \(2016\)](#). The rate constants for type 1 are indeed higher than those for type 2 for reactions with FA, GX, and GA, but MF is a special case. Similarly for type 4, where the activation energies are higher than for type 2 and consequently the rate constants are lower for GA, but

again reaction MF2 deviates. At temperatures below 200 K the reaction rate constant for MF2 crosses first that of MF4 and later that of MF1 even though the barrier is higher. The origin of this behavior lies in the barrier width. Tunneling namely depends both on the barrier height and width as well as on the effective mass of the system. The narrower the barrier at low-energy incidence, the more tunneling may be expected. This can be visualized with the help of intrinsic reaction coordinates (IRCs). The IRC curves are presented in Fig. 6, note that these do not include ZPE corrections and therefore relate to the barrier height ΔE^\ddagger of Table 1.

Finally, it cannot be said that in general addition is more efficient than abstraction or vice versa, *e.g.*, compare reaction types 1 and 2 against 3, 4, and 6.

4.2 Reactions between FA and CH_nO

At decreasing temperatures tunneling dominates a reaction more and more. This can explain the large difference between the low temperature value for the rate constant of reaction FAR2 compared to FAR1. For FAR2 a C–O bond is formed and as heavy-atom tunneling is less efficient than hydrogen atom tunneling, the rate constant is much lower than what would be expected from the barrier height only (compare for instance MF4, GA6, and FAR2). Similarly for the reaction of FA with HCO, where a C–C bond is formed (FAR3), again the low-temperature rate constant is very low. Note also the lower values for the crossover temperatures of FAR2 and FAR3 compared to the hydrogen transfer reactions, indicating that tunneling also sets in at lower temperatures. Comparing the rate constant to the typical value assumed for radical-radical barrierless reactions, $\sim 10^{12} \text{ s}^{-1}$, it is clear that these reactions are much less likely to contribute to COM formation. On that note we do wish to stress, however, to keep in mind that although radical-radical reactions may be able to proceed without a barrier, this does not mean that all reaction pathways are open, see for instance [Lamberts \(2018\)](#).

5 ASTROCHEMICALLY RELEVANT CONCLUSIONS

Unimolecular reaction rate constants have been calculated and are provided for hydrogen addition and abstraction reactions from methylformate, glyoxal, glycoaldehyde, and ethylene glycol and are thus available to be implemented in both rate-equation and kinetic Monte Carlo models aimed at studying the formation of COMs at low temperatures.

Our results are generally in agreement with experimental work, although some discrepancies exist on the efficiency of specific reaction paths, such as the formation of CH₂OH or CH₃O after hydrogen abstraction from methanol, which impacts on the ease of methylformate formation (for which CH₃O is needed) or ethylene glycol formation (for which CH₂OH is required). A microscopic model aiming to reproduce experiments may be able to provide a clear picture of how the reactions are intertwined with each other.

The reaction $\text{H} + \text{GX} \longrightarrow (\text{CO})\text{CHO} + \text{H}_2$ could not be studied and thus deserves further attention.

We found that one cannot predict average rate constants solely based on the type of the reaction. The spread in

the low-temperature rate constant can be roughly 7 orders of magnitude for a single reaction type (*e.g.*, hydrogen addition to an aldehyde carbon) showing a strong dependence on the other functional groups that are attached to the carbon backbone.

Within a single molecule, on the other hand, one can loosely say that hydrogen abstraction from an aldehyde group is faster than hydrogen addition to the same carbon. Both of these have a rate constant that is larger than hydrogen abstraction from a methyl group.

Care should be taken with extrapolating rate constants based on the height of the barrier alone, as calculations show that reactions with narrow barriers can have rate constants at low temperature that are higher than those with a lower activation energy.

Reactions that include the breakage or formation of a bond between two heavy atoms generally have low-temperature rate constants that are much lower than those for hydrogen addition or abstraction reactions as a result of the low efficiency of tunneling when heavy atoms are involved.

ACKNOWLEDGEMENTS

The authors acknowledges support for computer time by the state of Baden-Württemberg through bwHPC and the Germany Research Foundation (DFG) through grant no. INST 40/467-1FUGG and SFB 716/C.6. This project was financially supported by the European Union's Horizon 2020 research and innovation programme (grant agreement No. 646717, TUNNELCHEM), the Alexander von Humboldt Foundation, the Netherlands Organisation for Scientific Research (NWO) via a VENI fellowship (722.017.008) and the COST Action CM1401 via an STSM travel grant.

REFERENCES

- Adler T. B., Knizia G., Werner H.-J., 2007, *J. Chem. Phys.*, 127, 221106
- Affleck I., 1981, *Phys. Rev. Lett.*, 46, 388
- Althorpe S. C., 2011, *J. Chem. Phys.*, 134, 114104
- Álvarez-Barcia S., Flores J. R., Kästner J., 2014, *J. Phys. Chem. A*, 118, 78
- Andersson S., Goumans T. P. M., Arnaldsson A., 2011a, *Chem. Phys. Lett.*, 513, 31
- Andersson S., Goumans T., Arnaldsson A., 2011b, *Chemical Physics Letters*, 513, 31
- Bacmann A., Taquet V., Faure A., Kahane C., Ceccarelli C., 2012, *A&A*, 541, L12
- Balucani N., Ceccarelli C., Taquet V., 2015, *Mon. Not. R. Astron. Soc. Lett.*, 449, L16
- Belloche A., Müller, H. S. P. Garrod, R. T. Menten, K. M. 2016, *A&A*, 587, A91
- Benderskii V. A., Makarov D. E., Wight C. A., 1994, *Adv. Chem. Phys.*, 88, 55
- Boogert A. A., Gerakines P. A., Whittet D. C., 2015, *Ann. Rev. Astron. Astrophys.*, 53, 541
- Bottinelli S., et al., 2004, *Astrophys. J.*, 615, 354
- Butscher T., Duvernay F., Theule P., Danger G., Carissan Y., Hagebaum-Reignier D., Chiavassa T., 2015, *MNRAS*, 453, 1587
- Butscher T., Duvernay F., Rimola A., Segado-Centellas M., Chiavassa T., 2017, *Phys. Chem. Chem. Phys.*, 19, 2857
- Callan Jr. C. G., Coleman S., 1977, *Phys. Rev. D*, 16, 1762
- Chuang K.-J., Fedoseev G., Ioppolo S., van Dishoeck E. F., Linnartz H., 2016, *MNRAS*, 455, 1702
- Chuang K.-J., Fedoseev G., Qasim D., Ioppolo S., van Dishoeck E. F., Linnartz H., 2017, *MNRAS*, 467, 2552
- Coleman S., 1977, *Phys. Rev. D*, 15, 2929
- Coleman S., 1988, *Nucl. Phys. B*, 298, 178
- Coutens A., Viti S., Rawlings J. M. C., Beltrán M. T., Holdship J., Jiménez-Serra I., Quénard D., Rivilla V. M., 2018, *Mon. Not. R. Astron. Soc.*, 475, 2016
- Deegan M. J. O., Knowles P. J., 1994, *Chem. Phys. Lett.*, 227, 321
- Fedoseev G., Cuppen H. M., Ioppolo S., Lamberts T., Linnartz H., 2015, *MNRAS*, 448, 1288
- Fedoseev G., Chuang K.-J., Ioppolo S., Qasim D., van Dishoeck E. F., Linnartz H., 2017, *ApJ*, 842, 52
- Fuchs G. W., Cuppen H. M., Ioppolo S., Romanzin C., Bisschop S. E., Andersson S., van Dishoeck E. F., Linnartz H., 2009, *A&A*, 505, 629
- Garrod R. T., Widicus Weaver S. L., Herbst E., 2008, *ApJ*, 682, 283
- Gildener E., Patrascioiu A., 1977, *Phys. Rev. D*, 16, 423
- Gillan M. J., 1987, *J. Phys. C*, 20, 3621
- Goumans T. P. M., 2011a, *Mon. Not. R. Astron. Soc.*, 413, 26150
- Goumans T. P. M., 2011b, *Mon. Not. R. Astron. Soc.*, 415, 3129
- Goumans T. P. M., Kästner J., 2011, *The Journal of Physical Chemistry A*, 115, 10767
- Halfen D. T., Ilyushin V. V., Ziurys L. M., 2015, *ApJ*, 812, L5
- Hänggi P., Talkner P., Borkovec M., 1990, *Rev. Mod. Phys.*, 62, 251
- Hiraoka K., Miyagoshi T., Takayama T., Yamamoto K., Kihara Y., 1998, *Astrophys. J.*, 498, 710
- Jørgensen J. K., Favre C., Bisschop S. E., Bourke T. L., van Dishoeck E. F., Schmalzl M., 2012, *ApJ*, 757, L4
- Kästner J., Carr J. M., Keal T. W., Thiel W., Wander A., Sherwood P., 2009, *J. Phys. Chem. A*, 113, 11856
- Keller H., Floethmann H., Dobbyn A. J., Schinke R., Werner H., Bauer C., Rosmus P., 1996, *J. Chem. Phys.*, 105, 4983
- Knizia G., Adler T. B., Werner H.-J., 2009, *J. Chem. Phys.*, 130, 054104
- Knowles P. J., Hampel C., Werner H.-J., 1993, *J. Chem. Phys.*, 99, 5219
- Knowles P. J., Hampel C., Werner H.-J., 2000, *J. Chem. Phys.*, 112, 3106
- Kryvohuz M., 2011, *J. Chem. Phys.*, 134, 114103
- Kryvohuz M., 2014, *J. Phys. Chem. A*, 118, 535
- Lamberts T., 2018, acc. *Astron. Astrophys. Lett.*
- Lamberts T., Kästner J., 2017a, *J. Phys. Chem. A*, 121, 9736
- Lamberts T., Kästner J., 2017b, *ApJ*, 846, 43
- Langer J. S., 1967, *Ann. Phys. (N.Y.)*, 41, 108
- Langer J. S., 1969, *Ann. Phys. (N.Y.)*, 54, 258
- Lee T. J., 2003, *Chem. Phys. Lett.*, 372, 362
- Li X., Xu X., You X., Truhlar D. G., 2016, *The Journal of Physical Chemistry A*, 120, 4025
- Li J., et al., 2017, *Astrophys. J.*, 849, 115
- López-Sepulcre A., et al., 2017, *A&A*, 606, A121
- M. J. Frisch G. W. T. e. a., 2009, Gaussian 09 Revision D.01
- Meisner J., Lamberts T., Kästner J., 2017, *ACS Earth Space Chem.*, 1, 399
- Messina M., Schenter G. K., Garrett B. C., 1995, *J. Chem. Phys.*, 103, 3430
- Metz S., Kästner J., Sokol A. A., Keal T. W., Sherwood P., 2014, *WIREs Comput. Mol. Sci.*, 4, 101
- Miller W. H., 1975, *J. Chem. Phys.*, 62, 1899
- Nagaoka A., Watanabe N., Kouchi A., 2005, *Astrophys. J. Lett.*, 624, L29
- Nagaoka A., Watanabe N., Kouchi A., 2007, *J. Phys. Chem. A*, 111, 3016

- Öberg K. I., Bottinelli S., Jørgensen J. K., van Dishoeck E. F., 2010, *ApJ*, **716**, 825
- Peterson K. A., Adler T. B., Werner H.-J., 2008a, *J. Chem. Phys.*, **128**, 084102
- Peterson K. A., Adler T. B., Werner H.-J., 2008b, *J. Chem. Phys.*, **128**, 084102
- Richardson J. O., 2016, *J. Chem. Phys.*, **144**, 114106
- Richardson J. O., Althorpe S. C., 2009, *J. Chem. Phys.*, **131**, 214106
- Rimola A., Taquet, Vianney Ugliengo, Piero Balucani, Nadia Ceccarelli, Cecilia 2014, *A&A*, **572**, A70
- Rivilla V. M., Beltrán M. T., Cesaroni R., Fontani F., Codella C., Zhang Q., 2017, *A&A*, **598**, A59
- Rommel J. B., Kästner J., 2011, *J. Chem. Phys.*, **134**, 184107
- Rommel J. B., Goumans T. P. M., Kästner J., 2011, *J. Chem. Theory Comput.*, **7**, 690
- Sherwood P., et al., 2003, *J. Mol. Struct. (THEOCHEM)*, **632**, 1
- Shiozaki T., Werner H.-J., 2011, *J. Chem. Phys.*, **134**, 184104
- Shiozaki T., Knizia G., Werner H.-J., 2011, *J. Chem. Phys.*, **134**, 034113
- Song L., Kästner J., 2017, *The Astrophysical Journal*, **850**, 118
- Taquet V., López-Sepulcre A., Ceccarelli C., Neri R., Kahane C., Charnley S. B., 2015, *ApJ*, **804**, 81
- Taquet V., Wirström E. S., Charnley S. B., Faure A., López-Sepulcre A., Persson C. M., 2017, *A&A*, **607**, A20
- Tielens A. G. G. M., Hagen W., 1982, *A&A*, **114**, 245
- Vastel C., Ceccarelli C., Lefloch B., Bachiller R., 2014, *ApJ*, **795**, L2
- Watanabe N., Kouchi A., 2002, *ApJ*, **571**, L173
- Weigend F., 2006, *Phys. Chem. Chem. Phys.*, **8**, 1057
- Weigend F., Ahlrichs R., 2005, *Phys. Chem. Chem. Phys.*, **7**, 3297
- Woods P. M., Kelly G., Viti S., Slater B., Brown W. A., Puletti F., Burke D. J., Raza Z., 2012, *ApJ*, **750**, 19
- Zhao Y., Truhlar D. G., 2004, *J. Phys. Chem. A*, **108**, 6908

APPENDIX A: BENCHMARK CALCULATIONS

RHF-UCCSD(T)-F12/VTZ-F12//MPWB1K/def2-TZVP single-point energy calculations were performed in order to check if MPWB1K provides a suitable description of the energy landscape for the reactions studied here. In general, the CCSD(T)-F12 method can be seen as the gold standard for obtaining relative energies for systems that are well-described by a single reference wavefunction. This is typically assumed to be the case when the so-called T1 and D1 diagnostics are smaller than the commonly used threshold values ($T1 \leq 0.02$ and $D1 \leq 0.05$) (Lee 2003). Here, this is the case for reactions MF2, MF4, GX1, GA1, GA4, and EG4. These reactions are included in Table A1 and the deviation in the activation energy ranges between 0.4 and 3.3 kJ/mol, *i.e.*, within chemical accuracy.

Furthermore, the extent of the multireference character for reaction type 2 (MF2, GX2 and GA2) was tested via MRCI-F12/VTZ-F12//MPWB1K/def2-TZVP calculations (Shiozaki et al. 2011; Shiozaki & Werner 2011; Peterson et al. 2008a) for a reaction of the same type, but with a smaller reactant: $\text{H} + \text{H}_2\text{CO} \rightarrow \text{CH}_2\text{OH}$. These single-point energy calculations indicate that the reaction does not have a large multireference character. Firstly, the CI coefficients for the reference wavefunction of the transition state structure correspond to 0.934, -0.124, 0.074 and -0.051. In addition, the activation energies at DFT, CCSD(T)-F12 and MRCI-F12 level are similar (38.8, 40.6 and 36.4 kJ/mol, respectively). Therefore, here the CCSD(T)-F12 method is consid-

Table A1. Activation energies without zero-point energy correction (ΔE^\ddagger) with respect to the separated reactants (in kJ mol^{-1}) computed at the MPWB1K/def2-TZVP level (DFT) and RHF-UCCSD(T)-F12/VTZ-F12//MPWB1K/def2-TZVP (CC)

	ΔE^\ddagger DFT	ΔE^\ddagger CC
MF2	58.8	59.2
MF3	46.5	48.3 ^a
MF4	51.1	52.8
GX1	14.7	15.4
GX2	29.7	31.9 ^a
GA1	18.5	17.5
GA2	38.2	37.7 ^a
GA4	26.5	29.5
EG4	27.9	31.2

^a Single-reference character confirmed, see text

ered to be a reasonable reference method for these specific three reactions as well, *i.e.*, for a H addition to an aldehyde oxygen.

The MPWB1K functional has been shown to provide a good description for 9 out of the 17 reactions dealt with here, with reaction types 1 to 4 being included in this benchmark. Therefore, we assume that the other 8 reactions, including reaction type 5 and 6, can also be described with the same functional and basis set combination. As a double-check we have tested several functionals suggested by Li et al. (2016) to make sure that the activation energies obtained are of the correct magnitude, see Table A2.

APPENDIX B: RATE CONSTANTS

Tables B1-B5 give the values for the unimolecular reaction rate constants as calculated with instanton theory and corresponding to Figs. 2-5 and 7 of the main manuscript.

This paper has been typeset from a $\text{\TeX}/\text{\LaTeX}$ file prepared by the author.

Table A2. Activation energies without zero-point energy correction (ΔE^\ddagger) with respect to the separated reactants (in kJ mol^{-1}) computed with several functionals and the def2-TZVP basis set

	MPWB1K	M06-2X	MPW1B95	MN12-SX	N12-SX	SOGGA11-X
H + MF						
MF1	38.0	39.2	35.0	33.7	43.1	39.1
MF2	58.8	57.1	52.0	56.7	59.3	61.3
MF3	46.5	50.5	38.0	43.3	43.5	46.2
MF4	51.1	55.1	44.3	50.1	48.7	52.5
MF5	145.8	138.0	131.5	142.3	137.6	148.1
H + GX						
GX1	14.7	17.0	12.9	8.3	21.9	15.7
GX2	29.7	33.1	24.5	24.3	32.2	30.1
H + GA						
GA1	18.5	18.0	16.8	11.3	27.4	20.0
GA2	38.2	36.9	32.4	35.8	42.3	39.8
GA3	23.8	28.4	16.1	20.9	24.8	23.1
GA4	26.5	32.4	20.1	26.7	28.3	27.0
GA6	55.4	59.3	45.7	50.5	51.9	52.8
H + EG						
EG4	27.9	33.2	21.0	29.0	28.1	29.2
EG6	53.5	57.8	44.4	49.6	50.7	51.3

Table B1. Unimolecular reaction rate constants (k (s^{-1})) for reaction MF + H. The instanton path was discretised using 80 images.

T(K)	MF1	MF2	MF3	MF4	MF5
75	3.60E-01	1.75E+00		1.13E-01 ^b	3.77E-33
80			3.37E+00 ^a	1.38E-01 ^a	
85	4.80E-01	1.86E+00	4.16E+00 ^a	1.61E-01 ^a	1.70E-32
90	5.72E-01	1.90E+00	5.20E+00 ^a	1.87E-01 ^a	8.08E-32
95	6.91E-01	2.08E+00	6.47E+00 ^a	2.25E-01 ^a	1.78E-31
100			8.23E+00 ^a	2.79E-01	
105	1.02E+00	2.54E+00	1.12E+01	3.76E-01	1.95E-30
110			1.41E+01	4.66E-01	
120			2.29E+01	7.50E-01	
130			3.77E+01	1.24E+00	
140	5.56E+00	5.60E+00	6.22E+01	2.08E+00	1.31E-26
150			1.03E+02		
160			1.70E+02		
170	2.80E+01	1.66E+01	2.78E+02	1.04E+01	2.73E-23
200	1.61E+02	5.11E+01	1.15E+03	4.93E+01	3.13E-20
250	3.80E+03	3.53E+02	9.31E+03	5.45E+02	6.43E-16
300		2.66E+03	6.22E+04	5.35E+03	1.72E-12
350		2.03E+04	3.70E+05		9.58E-10

^a 158 images

^b 314 images

Table B2. Unimolecular reaction rate constants (k (s^{-1})) for reaction GX + H. The instanton path was discretised using 80 images.

T(K)	GX1	GX2
75	9.62E+06	1.81E+03
85	1.02E+07	2.27E+03
90	1.16E+07	2.39E+03
95	1.33E+07	2.56E+03
105	1.76E+07	3.45E+03
140	6.97E+07	9.85E+03
170	2.88E+08	2.69E+04
200		7.55E+04
250		4.44E+05

Table B3. Unimolecular reaction rate constants (k (s^{-1})) for reaction GA + H. The instanton path was discretised using 80 images.

T(K)	GA1	GA2	GA3	GA4	GA6
75	2.78E+05	2.77E+02	6.83E+07	2.56E+04	9.61E-01
85	3.00E+05	1.90E+02	7.84E+07	3.23E+04	1.37E+00
90	3.22E+05	1.97E+02	8.66E+07	3.63E+04	1.36E+00
95	3.56E+05	2.24E+02	9.74E+07	4.13E+04	1.45E+00
105	4.62E+05	3.04E+02	1.26E+08	5.48E+04	1.85E+00
140	1.91E+06	1.07E+03	3.70E+08	1.57E+05	7.40E+00
170	7.83E+06	2.68E+03	9.96E+08	4.04E+05	2.77E+01
200		7.12E+03	2.72E+09	1.02E+06	9.41E+01
250		4.37E+04	1.26E+10	4.34E+06	6.25E+02
300		2.96E+05	3.96E+10	1.54E+07	4.16E+03
350					2.74E+04

Table B4. Unimolecular reaction rate constants (k (s^{-1})) for reaction EG + H. The instanton path was discretised using 80 images.

T(K)	EG4	EG6
75	3.47E+06	
85	4.60E+06	
90	5.46E+06	2.24E+03
95	6.20E+06	2.13E+03
105	7.48E+06	2.25E+03
140	2.73E+07	6.30E+03
170	7.54E+07	1.72E+04
200	2.28E+08	4.63E+04
250	1.02E+09	2.15E+05
300		1.11E+06
350		5.98E+06

Table B5. Unimolecular reaction rate constants (k (s^{-1})) for FA reactions. The instanton path was discretised using 80 images.

T(K)	FAR1	FAR2
50	1.99E+03	
55	2.29E+03	
65	3.16E+03	4.59E-09
75	4.89E+03	1.03E-08
85	7.87E+03	3.51E-08
90	9.93E+03	2.58E-07
95	1.26E+04	1.88E-07
105	2.13E+04	1.26E-06
140	1.24E+05	6.05E-04
170	5.77E+05	
200	2.63E+06	
250	2.99E+07	
300	2.62E+08	